Proceedings

Differentially rotating relativistic stars beyond the j-constant law

Panagiotis Iosif [1,‡] and Nikolaos Stergioulas [1,‡]*

[1] Department of Physics, Aristotle University of Thessaloniki, Thessaloniki 54124, Greece
* Correspondence: piosif@auth.gr (P.I); niksterg@auth.gr (N.S.)
‡ These authors contributed equally to this work.

Version February 1, 2021 submitted to Proceedings

Abstract: The merger of a binary neutron star (BNS) system can lead to different final states, depending on the total mass of the binary and the equation of state (EOS). One of the possible outcomes of the merger is a long-lived (lifetime > 10ms), compact and differentially rotating remnant. The Komatsu, Eriguchi and Hachisu (1989) differential rotation law (KEH) has been used almost exclusively in the literature to describe such configurations, despite the tension with corresponding rotational profiles reported from numerical simulations. New rotation laws suggested by Uryu et al. (2017) aspire to ease this tension and provide more realistic choices to describe the rotational profiles of BNS merger remnants. We have recently started constructing equilibrium models with one of the new rotation laws proposed, and comparing their physical properties to the KEH rotation law counterpart models. In addition, building on earlier work, the accuracy of the IWM-CFC conformal flatness approximation with the new differential rotation law has been confirmed.

Keywords: general relativity; neutron stars; differential rotation; conformal flatness

1. Introduction

Differential rotation in relativistic stars has drawn a steady research interest because it is relevant in phenomena such as binary neutron star (BNS) mergers that can provide information through gravitational and electromagnetic waves observations for the behaviour of matter at high densities, i.e. the equation of state (EOS). More specifically, if the total mass M of the BNS is greater than the maximum mass of a cold, uniformly rotating neutron star, $M_{\rm max,rot}$, then the compact remnant that is formed during the merger can survive for several tens of milliseconds (ms) supported by differential rotation and thermal pressure. Oscillations of the post-merger remnant could lead to tight constraints for the EOS in case of detection of one (or more) of three observable frequencies ($f_{\rm peak}$, f_{2-0}, $f_{\rm spiral}$) [1–4].

While numerical simulations are used primarily to study BNS mergers, their high computational cost calls for complementary approaches, such as equilibrium modelling in order to allow for faster and wider parameter space exploration. In the equilibrium framework, several aspects of the merger remnant are neglected in order to obtain idealized models of its structure. Enriching these initial idealized models by adding gradually, selected realistic components of the binary coalescence problem ensures that this method can still provide useful insights.

Concerning the differential rotation aspect of the BNS merger problem, the simple solution that was adopted for years in the relevant literature was the rotation law

$$F(\Omega) = A^2(\Omega_c - \Omega) \tag{1}$$

by [5] (hereafter KEH), where A is a positive constant that determines the length scale over which the angular velocity Ω varies within the star, Ω_c is the angular velocity at the rotation axis and $F = u^t u_\phi$

denotes the gravitationally redshifted angular momentum per unit rest mass and enthalpy. Limiting cases of the rotation law (1) are the uniform rotation case for $A \to \infty$ and the j-constant law for $A \to 0$ (where $j = hu_\phi$ is the specific angular momentum).

More realistic rotation laws have been proposed [6], that better describe a remnant's rotational profile as reported from simulations (e.g. see [7] for a recent study). In our recent work [8], we investigate one of the new rotation laws, compare physical properties of constructed models with the "classic" KEH law to the new law and verify its suitability to describe BNS merger remnants.

2. Methods

Within the framework of full general relativity (GR), in [8] we construct stationary and axisymmetric stellar configurations in equilibrium, described by the line element:

$$ds^2 = -e^{\gamma+\rho}dt^2 + e^{\gamma-\rho}r^2\sin^2\theta(d\phi - \omega dt)^2 + e^{2\mu}(dr^2 + r^2 d\theta^2)\,, \tag{2}$$

with γ, ρ, ω and μ being metric functions that depend only on the coordinates r and θ. Matter is described as a perfect fluid, assuming a polytropic EOS:

$$p = K\rho^{1+\frac{1}{N}}\,, \tag{3}$$

where p is the pressure, ρ is the rest mass density, K is the polytropic constant and N is the polytropic index (see [9] for details). We choose $N = 1$ and $K = 100$, which is a common choice in the literature for testing numerical codes. We note that a polytropic model is calculated with $K = 1$ and then rescaled to $K = 100$ (or any other choice of K) by multiplying with appropriate factors [10].

In order to create our equilibrium models we use an extended version [11,12] of the public domain `rns` code [13,14]. The code is based on the KEH scheme [5] and includes modifications by [10]. We expanded the code in order to implement the 4-parameter rotation law introduced in [6]

$$\Omega = \Omega_c \frac{1 + \left(\dfrac{F}{B^2\Omega_c}\right)^p}{1 + \left(\dfrac{F}{A^2\Omega_c}\right)^{q+p}}\,, \tag{4}$$

(hereafter Uryu+ law). The parameter p controls the growth of the rotation curve near the rotation axis and parameter q controls the asymptotic behavior of $\Omega(r)$. Setting $q = 3$ recovers the Keplerian rotation law in the Newtonian limit. In Figure 1 we present an example of the angular velocity profile in the equatorial plane, for the Uryu+ rotation law (4).

We choose the values $\{p, q\} = \{1, 3\}$, for which the integral in the hydrostationary equilibrium expression has an analytic solution. The parameters A and B are determined by solving for them in each iteration, via fixing the ratios of the maximum angular velocity over the angular velocity at the center of the configuration, $\lambda_1 = \Omega_{\max}/\Omega_c$, and of the angular velocity at the equator over the angular velocity at the center, $\lambda_2 = \Omega_e/\Omega_c$, to certain selected values [6,15]. As reference values for the ratios $\{\lambda_1, \lambda_2\}$ we adopt the choice $\{2.0, 0.5\}$ as in [6]. However, differences in rotational profiles seen in numerical simulations of post-merger remnants, when different EOS and total masses are used [7,16] provides motivation to examine two values for the first parameter $\lambda_1 = \{2.0, 1.5\}$ and two values for the second parameter $\lambda_2 = \{0.5, 1.0\}$, leading to four distinct pairs of $\{\lambda_1, \lambda_2\}$.

3. Results

For comparison with previous work [11,17] employing the KEH differential rotation law, in [8] we construct three sequences of equilibrium models using the new differential rotation law (4):

- Sequence A is a constant rest mass sequence with $M_0 = 1.506$.
- Sequence B is a constant central energy density sequence with $\epsilon_c = 1.444 \times 10^{-3}$.
- Sequence C is a constant central energy density sequence with $\epsilon_c = 3.3 \times 10^{-3}$.

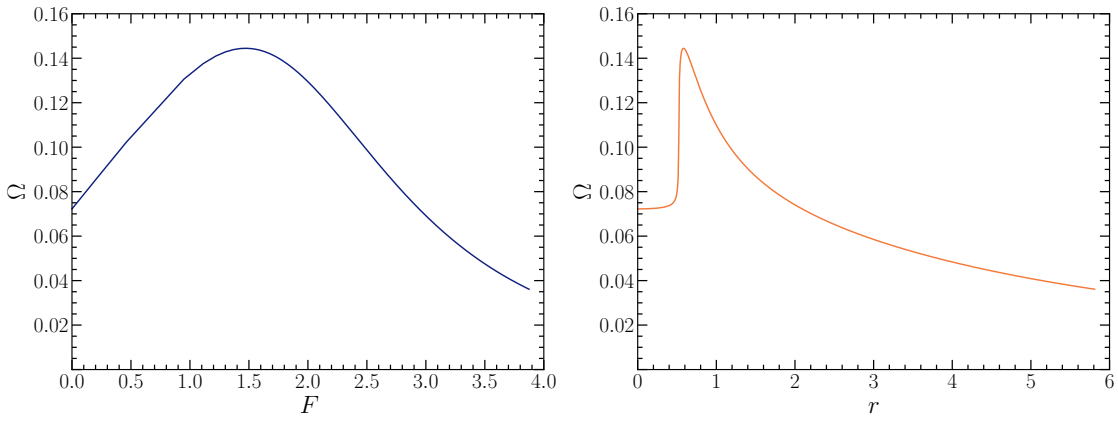

Figure 1. Angular velocity Ω profiles in the equatorial plane for model C6 (axis ratio r_p/r_e = 0.43), constructed with the Uryu+ rotation law with $\{\lambda_1, \lambda_2\} = \{2.0, 0.5\}$ (see Section 3 for details). (**a**) left panel: plotted versus the gravitationally redshifted angular momentum per unit rest mass and enthalpy F. (**b**) right panel: plotted versus the coordinate radius r. Figure from [8].

Throughout the text we employ dimensionless units for all physical quantities by setting $c = G = M_\odot = 1$ (see also [10]). We note that the maximum mass nonrotating model for our chosen EOS has a central energy density $\epsilon_c = 4.122 \times 10^{-3}$, with a gravitational mass of $M \simeq 1.64$ and a rest mass of $M_0 \simeq 1.8$. Figure 2 acts as an illustrated definition of equilibrium sequences A, B and C.

We perform a comparison between the new Uryu+ rotation law and the KEH law and verify a close agreement for the masses of the corresponding configurations. The left panel of Figure 3 shows a difference at the 1% level for low density and rapidly rotating models, that becomes much smaller as the compactness increases for sequences B and C (right panel). There is a slightly larger influence of the rotation law choice on the radius, as smaller radii are found for the Uryu+ models. This is attributed to a weaker centrifugal force in the Uryu+ models, since the angular velocities at the equator Ω_e were also found to be smaller. We note that results shown in Figure 3 are obtained with the reference values $\{\lambda_1, \lambda_2\} = \{2.0, 0.5\}$.

In order to highlight the distinction between quasi-toroidal and quasi-spheroidal morphologies we explore additional values of parameters $\{\lambda_1, \lambda_2\}$ for a representative model with $r_p/r_e = 0.5$ (Figure 4). From the four pairs of $\{\lambda_1, \lambda_2\}$ values considered, only the pair $\{2.0, 0.5\}$ leads to a quasi-toroidal configuration. This is consistent with the corresponding $\Omega(r)$ profile having the highest degree of differential rotation (right panel of Figure 4). Similar results are obtained with corresponding models with $r_p/r_e \sim 0.5$ from sequences A and C. We go on to construct full sequence C variations (i.e. of constant central energy density $\epsilon_c = 3.3 \times 10^{-3}$) with the Uryu+ rotation law but different $\{\lambda_1, \lambda_2\}$ values. The $M(R_e)$ curves in Figure 5 summarize the four equilibrium variation sequences (extra equilibrium solutions were calculated for Figure 5, in order to produce smoother curves).

A mass-shedding limit is found for the cases $\{\lambda_1, \lambda_2\} = \{2.0, 1.0\}$ and $\{1.5, 1.0\}$ at axis ratio values of 0.38602 and 0.46693 respectively. This classifies these sequences as type A solutions according to [18]. For the cases $\{\lambda_1, \lambda_2\} = \{2.0, 0.5\}$ and $\{1.5, 0.5\}$, no mass-shedding limit is found. For the terminal models of the latter sequences, i.e. the highest mass models of the corresponding curves in Figure 5, the maximum density is located off-center and quasi-toroidal morphology has been established. The above characteristics classify these sequences as type C solutions according to [18].

As a worst case scenario, in [8] we also perform a comparison between full GR and the IWM-CFC conformal flatness approximation [19,20] for a representative model of our most compact sequence C with $r_p/r_e = 0.5$ for the highest degree of differential rotation considered here, i.e. $\{\lambda_1, \lambda_2\} = \{2.0, 0.5\}$. Figure 6 shows the energy density and angular velocity profiles of the specific model for the GR and IWM-CFC case. We find that the IWM-CFC approximation remains acceptably accurate for models with an axis ratio $r_p/r_e = 0.5$, than can be considered as merger-mimicking candidates. The relative

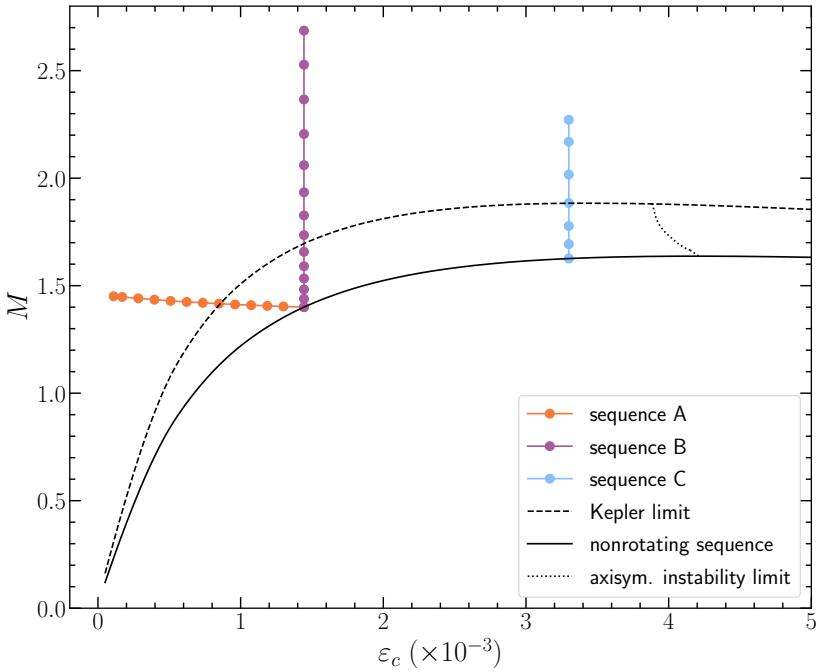

Figure 2. Gravitational mass M versus the central energy density ϵ_c for definition of sequences A, B and C. For reference the nonrotating (TOV) sequence (solid line), the mass-shedding (Kepler) limit for uniform rotation (dashed line) and the axisymmetric instability limit for uniform rotation (dotted line) are shown. Figure from [8].

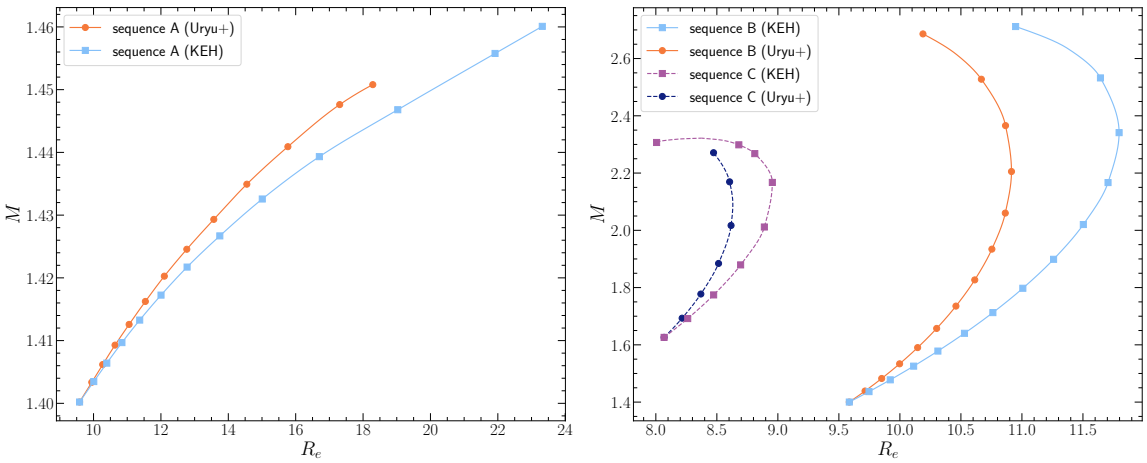

Figure 3. Comparison of the gravitational mass M versus the circumferential radius R_e for the equilibrium models of sequences A, B and C, constructed with the Uryu+ and the KEH differential rotation laws. The values $\{\lambda_1, \lambda_2\} = \{2.0, 0.5\}$ have been used for the Uryu+ law calculations. Figure from [8].

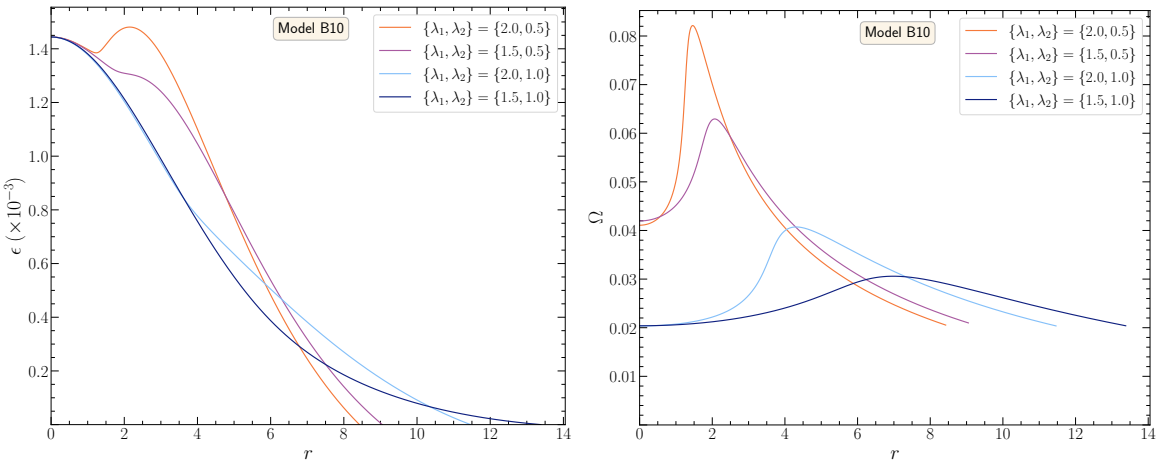

Figure 4. Effect of the different options for parameters $\{\lambda_1, \lambda_2\}$ for model B10 ($r_p/r_e = 0.5$). (**a**) left column: energy density profile $\epsilon(r)$ versus the coordinate radius r in the equatorial plane. (**B**) right column: angular velocity profile $\Omega(r)$ in the equatorial plane. Figure from [8].

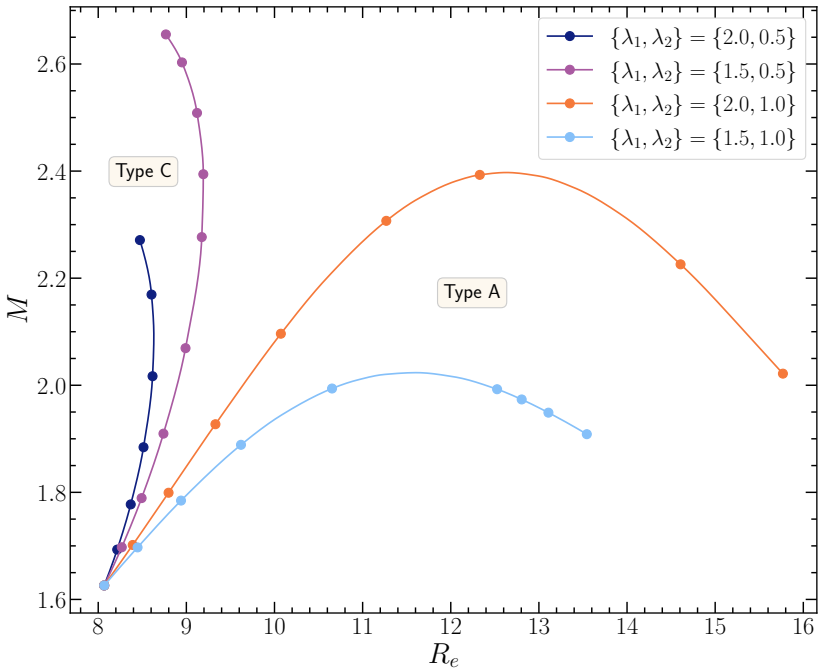

Figure 5. Gravitational mass M versus the circumferential radius R_e for the variations of sequence C, constructed with the Uryu+ differential rotation law and employing different $\{\lambda_1, \lambda_2\}$ values. Equilibrium models with $\{\lambda_1, \lambda_2\} = \{2.0, 0.5\}$ and $\{1.5, 0.5\}$ are type C solutions, while models with $\{\lambda_1, \lambda_2\} = \{2.0, 1.0\}$ and $\{1.5, 1.0\}$ are type A solutions [18]. Figure from [8].

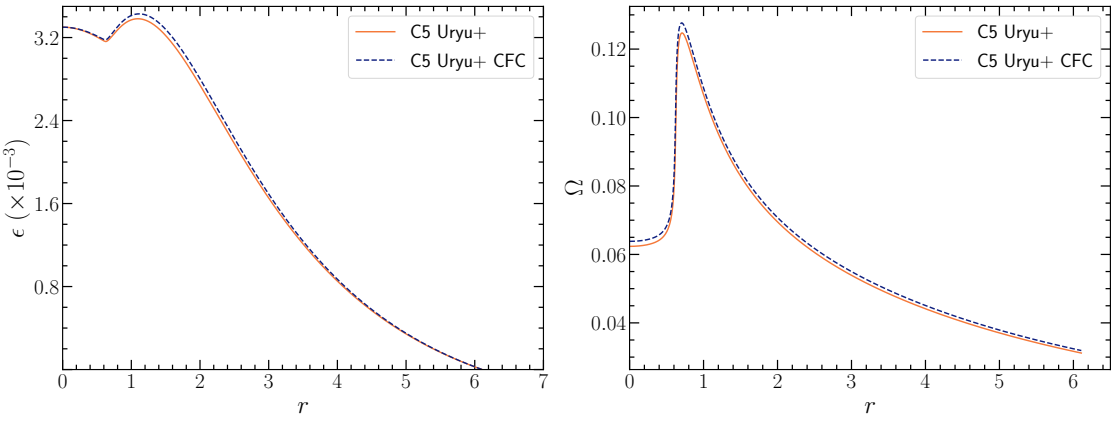

Figure 6. Comparison between full GR and the IWM-CFC approximation for model C5 ($r_p/r_e = 0.5$) calculated for the Uryu+ rotation law with $\{\lambda_1, \lambda_2\} = \{2.0, 0.5\}$. (**a**) left panel: energy density profile in the equatorial lane $\epsilon(r)$ versus the coordinate radius r. (**b**) right panel: angular velocity profile in the equatorial plane $\Omega(r)$ versus the coordinate radius r. Figure from [8].

errors for local quantities (such as the radius and the angular velocity) are up to $\sim 2.5\%$ and $\sim 1\%$ for the masses and the ratio $T/|W|$ of the rotational kinetic energy over the absolute value of the gravitational binding energy. This is consistent with the corresponding errors reported in [17] for the same sequence calculated with the KEH rotation law with $\hat{A} = 1$ (Figure 7).

4. Discussion

In [8] we found that the versatility of the new Uryu+ rotation law allows for construction of equilibrium solutions with a rotational profile much closer to the one observed for merger remnants in numerical simulations, while at the same time dwelling in the realm of type A solutions [18] (i.e. quasi-spherical). This is an important development towards constructing more realistic equilibrium models that can mimic the properties of merger remnants. Having more realistic models available will allow further insights about stellar stability and the threshold for prompt collapse to emerge in future studies. A necessary first step to that direction, is to expand this study for realistic and hot EOS. Recently, new multivariate, empirical relations were reported for the post-merger frequencies $f_{\rm peak}$ (the dominant oscillation frequency stemming from excitation of the fundamental quadrupolar $l = m = 2$ mode), $f_{\rm spiral}$ (stemming from a spiral deformation, the pattern of which rotates slower with respect to the double-core structure in the center of the remnant) and f_{2-0} (stemming from a non-linear coupling of the $m = 2$ mode to the fundamental quasi-radial $m = 0$ mode) [21]. Another interesting follow-up would be to study these oscillations and empirical relations using configurations constructed with the new Uryu+ law via time evolution or perturbation methods.

Funding: PI gratefully acknowledges support by a Virgo-EGO Scientific Forum (VESF) PhD fellowship.

Acknowledgments: We would like to thank Gabriele Bozzola and Wolfgang Kastaun for useful discussions. In addition, we thank Giovanni Camelio, Tim Dietrich, Stephan Rosswog and Bryn Haskell for advanced sharing of a manuscript on a related topic and for comments on our manuscript. The authors gratefully acknowledge the Italian Istituto Nazionale di Fisica Nucleare (INFN), the French Centre National de la Recherche Scientifique (CNRS) and the Netherlands Organization for Scientific Research, for the construction and operation of the Virgo detector and the creation and support of the EGO consortium.

Conflicts of Interest: The authors declare no conflict of interest.

Abbreviations

The following abbreviations are used in this manuscript:

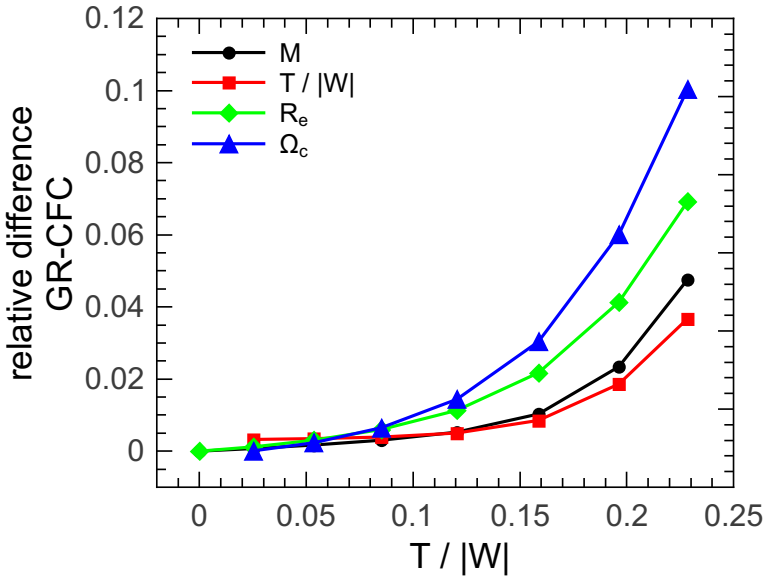

Figure 7. Absolute values of the relative difference between full GR and IWM-CFC approximation for the gravitational mass M, the ratio of rotational to gravitational binding energy $T/|W|$, the equatorial circumferential radius R_e and the angular velocity at the center of the configuration Ω_c for sequence C calculated with the KEH rotation law. Values at $T/|W| \sim 0.16$ correspond to an axis ratio $r_p/r_e = 0.5$. Figure from [17].

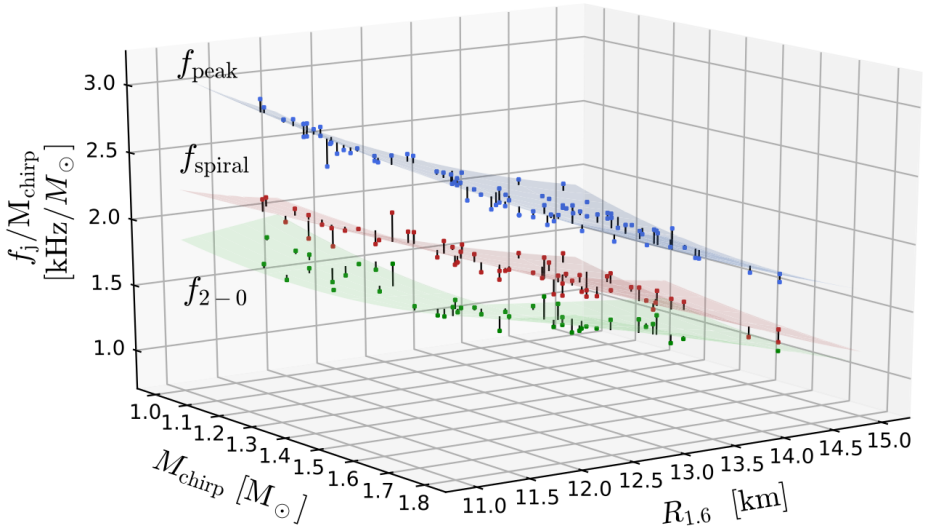

Figure 8. Surfaces corresponding to empirical relations for the three different post-merger frequencies $f_{\rm peak}$, $f_{\rm spiral}$ and f_{2-0}, as a function of the chirp mass $M_{\rm chirp}$ and the equatorial circumferential radius $R_{1.6}$ of a nonrotating model with gravitational mass $M = 1.6 M_\odot$. Figure from [21].

KEH	Komatsu, Eriguchi and Hachisu
EOS	equation of state
BNS	binary neutron star
IWM	Isenberg, Wilson, Mathews
CFC	conformal flatness condition
GR	general relativity

References

1. Stergioulas, N.; Bauswein, A.; Zagkouris, K.; Janka, H.T. Gravitational waves and non-axisymmetric oscillation modes in mergers of compact object binaries. *Mon. Not. R. Astron. Soc.* **2011**, *418*, 427–436. doi:10.1111/j.1365-2966.2011.19493.x.
2. Bauswein, A.; Stergioulas, N. Unified picture of the post-merger dynamics and gravitational wave emission in neutron star mergers. *Phys. Rev. D* **2015**, *91*, 124056. doi:10.1103/PhysRevD.91.124056.
3. Bauswein, A.; Stergioulas, N.; Janka, H.T. Exploring properties of high-density matter through remnants of neutron-star mergers. *Eur. Phys. J. A* **2016**, *52*, 56. doi:10.1140/epja/i2016-16056-7.
4. Bauswein, A.; Stergioulas, N. Spectral classification of gravitational-wave emission and equation of state constraints in binary neutron star mergers. *J. Phys. G: Nucl. Part. Phys.* **2019**, *46*, 113002. doi:10.1088/1361-6471/ab2b90.
5. Komatsu, H.; Eriguchi, Y.; Hachisu, I. Rapidly rotating general relativistic stars. I - Numerical method and its application to uniformly rotating polytropes. *Mon. Not. R. Astron. Soc.* **1989**, *237*, 355–379. doi:10.1093/mnras/237.2.355.
6. Uryū, K.; Tsokaros, A.; Baiotti, L.; Galeazzi, F.; Taniguchi, K.; Yoshida, S. Modeling differential rotations of compact stars in equilibriums. *Phys. Rev. D* **2017**, *96*, 103011. doi:10.1103/PhysRevD.96.103011.
7. De Pietri, R.; Feo, A.; Font, J.A.; Löffler, F.; Pasquali, M.; Stergioulas, N. Numerical-relativity simulations of long-lived remnants of binary neutron star mergers. *Phys. Rev. D* **2020**, *101*, 064052. doi:10.1103/PhysRevD.101.064052.
8. Iosif, P.; Stergioulas, N. Equilibrium sequences of differentially rotating stars with post-merger-like rotational profiles. *arXiv e-prints* **2020**, [arXiv:gr-qc/2011.10612].
9. Friedman, J.L.; Stergioulas, N. *Rotating Relativistic Stars*; Cambridge Monographs on Mathematical Physics, Cambridge University Press, 2013. doi:10.1017/CBO9780511977596.
10. Cook, G.B.; Shapiro, S.L.; Teukolsky, S.A. Spin-up of a Rapidly Rotating Star by Angular Momentum Loss: Effects of General Relativity. *Astrophys. J.* **1992**, *398*, 203. doi:10.1086/171849.
11. Stergioulas, N.; Apostolatos, T.A.; Font, J.A. Non-linear pulsations in differentially rotating neutron stars: mass-shedding-induced damping and splitting of the fundamental mode. *Mon. Not. R. Astron. Soc.* **2004**, *352*, 1089–1101. doi:10.1111/j.1365-2966.2004.07973.x.
12. Bauswein, A.; Stergioulas, N. Semi-analytic derivation of the threshold mass for prompt collapse in binary neutron-star mergers. *Mon. Not. R. Astron. Soc.* **2017**, *471*, 4956–4965. doi:10.1093/mnras/stx1983.
13. Stergioulas, N.; Friedman, J.L. Comparing Models of Rapidly Rotating Relativistic Stars Constructed by Two Numerical Methods. *Astrophys. J.* **1995**, *444*, 306. doi:10.1086/175605.
14. Stergioulas, N. RNS. http://www.gravity.phys.uwm.edu/rns. public domain code.
15. Zhou, E.; Tsokaros, A.; Uryū, K.; Xu, R.; Shibata, M. Differentially rotating strange star in general relativity. *Phys. Rev. D* **2019**, *100*, 043015. doi:10.1103/PhysRevD.100.043015.
16. Hanauske, M.; Takami, K.; Bovard, L.; Rezzolla, L.; Font, J.A.; Galeazzi, F.; Stöcker, H. Rotational properties of hypermassive neutron stars from binary mergers. *Phys. Rev. D* **2017**, *96*, 043004. doi:10.1103/PhysRevD.96.043004.
17. Iosif, P.; Stergioulas, N. On the accuracy of the IWM–CFC approximation in differentially rotating relativistic stars. *Gen. Relativ. Gravit.* **2014**, *46*, 1800. doi:10.1007/s10714-014-1800-5.
18. Ansorg, M.; Gondek-Rosińska, D.; Villain, L. On the solution space of differentially rotating neutron stars in general relativity. *Mon. Not. R. Astron. Soc.* **2009**, *396*, 2359–2366. doi:10.1111/j.1365-2966.2009.14904.x.
19. Isenberg, J.A. Waveless Approximation Theories of Gravity. *Int. J. Mod. Phys. D* **2008**, *17*, 265–273. doi:10.1142/S0218271808011997.

20. Wilson, J.R.; Mathews, G.J.; Marronetti, P. Relativistic numerical model for close neutron-star binaries. *Phys. Rev. D* **1996**, *54*, 1317–1331. doi:10.1103/PhysRevD.54.1317.
21. Vretinaris, S.; Stergioulas, N.; Bauswein, A. Empirical relations for gravitational-wave asteroseismology of binary neutron star mergers. *Phys. Rev. D* **2020**, *101*, 084039. doi:10.1103/PhysRevD.101.084039.